WP 1 DETECTOR DESIGN RECOMMENDATIONS

Authors: Workgroup 1 (Ilker Meric, Jarle R Sølie, Hesam Shafiee, Helge E S Pettersen)

The design recommendations on the Digital Tracking Calorimeter with ALPIDE sensor chips are based calculations on the following properties regarding proton tracking and reconstruction quality:

1. Range uncertainty (stochastic)
2. Range accuracy (systematic)
3. Tracking efficiency
4. Economy (number of layers)

The different properties have been calculated using the pCT software framework on different versions of the geometry as well as theoretical calculations.

This work is focused on finding the optimal spacing between the sensor layers in a range telescope for proton CT. By considering several different values for the spacing and carrying out the analysis as outlaid in the benchmarking of the proof-of-concept calorimeter, metrics such as range accuracy and range uncertainty are found for each of the designs.

MAIN FINDINGS

1. The lateral size of the sensor chips should be approximately 15 x 27 cm^2, depending mainly on the inherited design from the ITS from ALICE and comparisons with other proton CT projects. The added value of doubling the detector in vertical dimensions is small compared to the corresponding added accuracy of doubling the longitudinal number of layers: It is a software task of stitching two scans vertically. This corresponds to 90 ALPIDE chips per layer.

2. The longitudinal size of the detector should be so that the absorbing material (Al) is 3.5 mm thick. This value corresponds to 41 (41.1) layers being needed to fully contain a 230 MeV proton beam including 3 sigma range straggling. 41 x 90 = 3690 chips in total.

   Using this value, the added range uncertainty is 2 mm Water Equivalent Thickness (WET), compared to the range straggling of 3.8 mm WET that is added to this number in quadrature. The oscillating artifacts introduced in the range determination accuracy is kept below 0.1 mm WET. The track reconstruction efficiency (fraction of fully and correctly reconstructed proton tracks) increases rapidly with decreasing absorber thickness, and from this perspective the thickness should be kept below 4 mm and as low as possible.

3. Any material between the two first sensor layers, i.e. the aluminum carrier board, should be kept as thin as possible and below 0.45 mm. A thicker slab lead to higher amounts multiple Coulomb scattering, and positional errors on the phantom in excess of 0.5 mm.

METHODS

The goal of this study is to optimize the geometrical and material design of the DTC. The target for such a design is the simultaneous optimization of the following metrics: high accuracy of the range determination, limited by a non-existent systematic bias; low uncertainty (standard deviation) in the range determination, limited by the proton beam's range straggling; high track reconstruction efficiency, i.e. the ability to disentangle and reconstruct all the protons in a single readout frame; and secondary constraints such as economy (number of layers), cooling and mechanical stability.

Note that in order to obtain the best possible estimates of the performance of the different DTC designs, the different parts of the analysis are treated separately: The track reconstruction step is omitted during the evaluation of the residual range calculation, where the tracks are obtained directly from the MC truth.

Several geometrical configurations are needed to evaluate how the desired detector metrics: such as range accuracy, range uncertainty and track reconstruction efficiency, depends on the design. It is possible to define a large number of potential designs for the DTC, and some constraints must be put on the degrees of freedom. A baseline design based upon the original prototype of the tracking detector (Pettersen et al. 2017a) is shown in **Figure 1**: While the geometry of the sensor chips and electronic components are kept, the energy degrading part of the sampling calorimeter, here called the *absorbers*, are chosen to be between 2 mm and 6 mm of either aluminum or carbon. The proposed design use an upgraded sensor chip compared to the original prototype, and as such the detector thickness might be decreased.

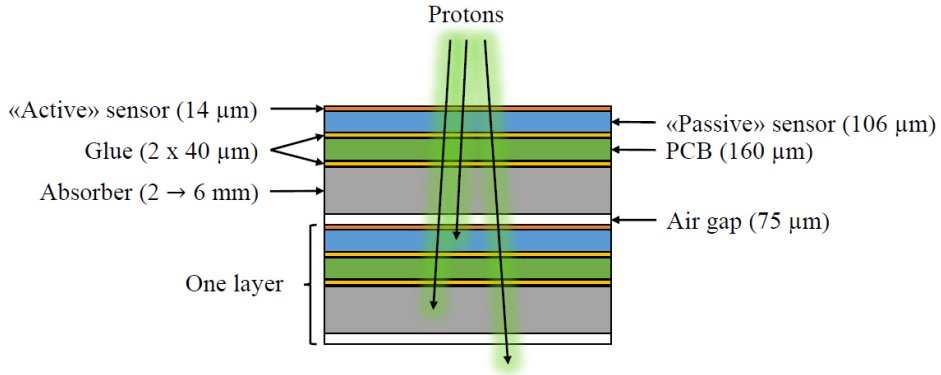

Figure 1: *Design to be optimized: Different thicknesses (2 to 6 mm) and materials (aluminum and carbon) for the energy absorbers are considered, and evaluated through the MC simulations. Only the "active" sensor part is readout in the MC simulations.*

A number of scenarios are defined by varying the thickness of an energy degrading water phantom whereas the GATE software has been configured for a single geometry configuration. This is used to modulate a monoenergetic 250 MeV beam to represent realistic energy spectra with residual ranges that span the complete DTC in depth. The water phantom thicknesses vary from 0 cm to the maximum water equivalent range of the beam, approximately 38 cm, in steps of 1 mm. This fine thickness segmentation has been chosen in order to characterize the linearity of the range determination accuracy. The beam is placed distal to the water phantom, uniformly distributed on a plane, with an area of 100 cm^2, parallel to the sensor area. In **Figure 2** the placement of the water phantom is shown.

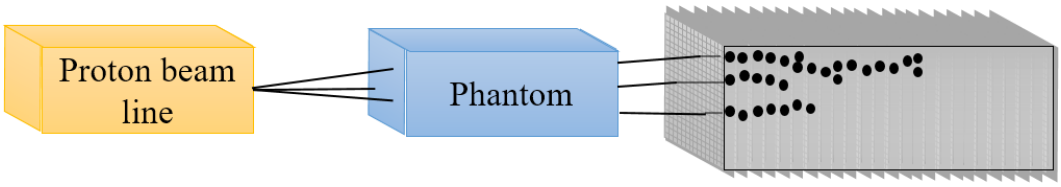

Figure 2: *Schematic setup of the variable geometry used for the design optimization. In order to obtain a spectrum of different proton beams to hit the DTC, the thickness of the energy degrading water phantom is modulated from 0 cm to the maximum range of the 250 MeV beam, which is approximately 38 cm.*

The final range calculations that emerge from the following sections need to be compared to a ground truth. For this purpose, separate MC calculations have been performed. A look-up-table between phantom thicknesses and residual DTC range is created, by using the geometrical input file as described above and recording the interactions in all volumes. This is repeated for all design variants and water phantom thicknesses. The look-up-table is then used in conjunction with spline interpolation, as this method was shown to be very accurate (Pettersen et al., 2017b).

A look-up-table for proton ranges in pure water is also created in order to calculate the Water Equivalent Thickness (WET) from a given proton range in the DTC: This is done by calculating the energy from the proton range, and then the WET from the energy. Note that this procedure is more accurate compared to using a constant stopping power ratio between water and the detector materials.

One of the strengths of the DTC design is its ability to untangle and reconstruct a large number of concurrent traversing proton tracks. To this end, a track reconstruction algorithm must be implemented. For more details on the track reconstruction applied in this context, see (Pettersen et al. 2017a).

It is possible to perform a least-squares fit of the Bragg Curve to the track's energy loss measurements in each sensor layer. This procedure increases the range determination accuracy compared to using the depth of the last recorded hit. While direct measurement of the energy loss is not possible using the proposed digital sensor readout ("hit" or "no hit"), it is possible to estimate the energy loss by counting the number of connected hits originating from the proton path, as described in detail in (Pettersen et al. 2017a), and as such this kind of model fitting is deemed appropriate.

The distribution of true proton ranges, having the same initial energy, is approximately gaussian. However, the output range distribution originating from the Bragg Curve fitting is not gaussian, and it is not trivial to describe the variations analytically due to the nature of the sparse measurements from each sensor layer. However, a simple histogram calculation of the empirical mean value and standard deviation yields accurate results for the residual range $\langle R_0 \rangle$ and range straggling $\langle \sigma \rangle$, respectively. The procedure is described in detail in (Pettersen et al. 2017a): A gaussian fit (μ', σ') to the whole range distribution histogram with bin heights (number of individual proton ranges) w_i and depth values x_i yields the summation limits for the bin counting from $x_1 = \mu' - 4\sigma'$ to $x_2 = \mu' + 4\sigma'$. Then,

$$\langle R_0 \rangle = \frac{\sum_{i=x_1}^{x_2} w_i x_i}{\sum_{i=x_1}^{x_2} w_i}, \qquad \langle \sigma \rangle = \sqrt{\frac{\sum_{i=x_1}^{x_2} w_i (x_i - \langle R_0 \rangle)^2}{\left[\sum_{i=x_1}^{x_2} w_i\right] - 1}}.$$

The results of these calculations should be comparable to the ground truth obtained from separate MC simulations. However, it is expected that the values should be degraded somewhat. First, in terms of a systematic error, or bias, leading to deviations in $\langle R_0 \rangle$ compared to the nominal residual range.

Second, in terms of an increase in the measurement uncertainty $\langle\sigma\rangle$ compared to the range straggling. These degradations may originate from the design of the DTC setup and from the data analysis procedure itself. By comparing the measured values to their ground truth counterparts, the bias in $\langle R_0 \rangle$ is trivial to calculate in different design scenarios.

RESULTS

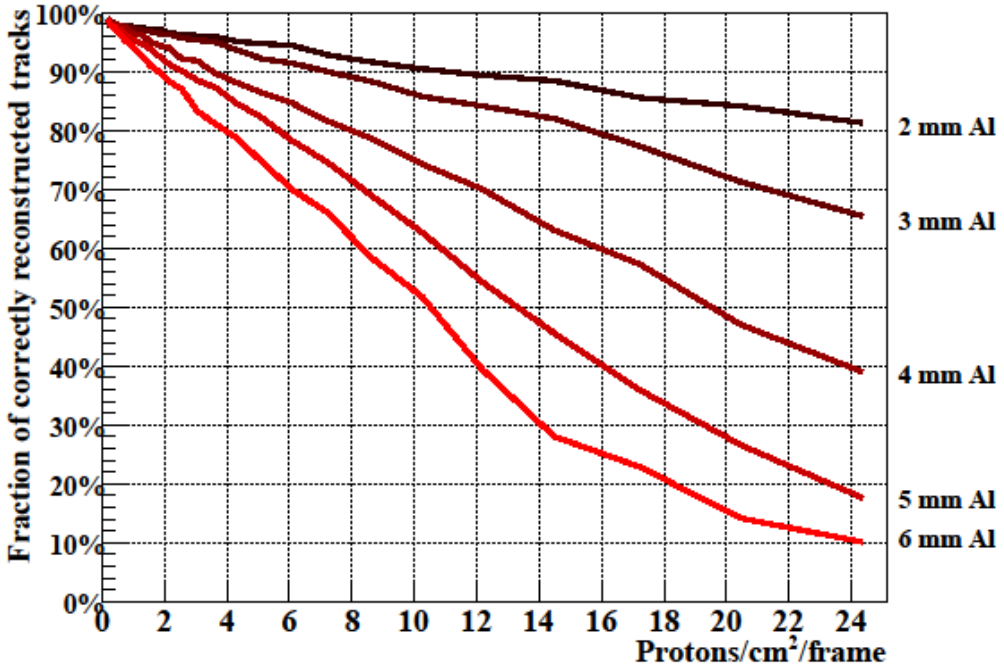

Figure 3: *The tracking efficiency for different geometries. Each proton track must be fully reconstructed, and the start- and endpoint must originate from the same incoming proton. Note that in many cases, the effect of a wrongly reconstructed track might be small due to the nature of the error: Parallel tracks originating from similar incoming vectors are easily confused. If such tracks were accepted the final tracking efficiency would be higher.*

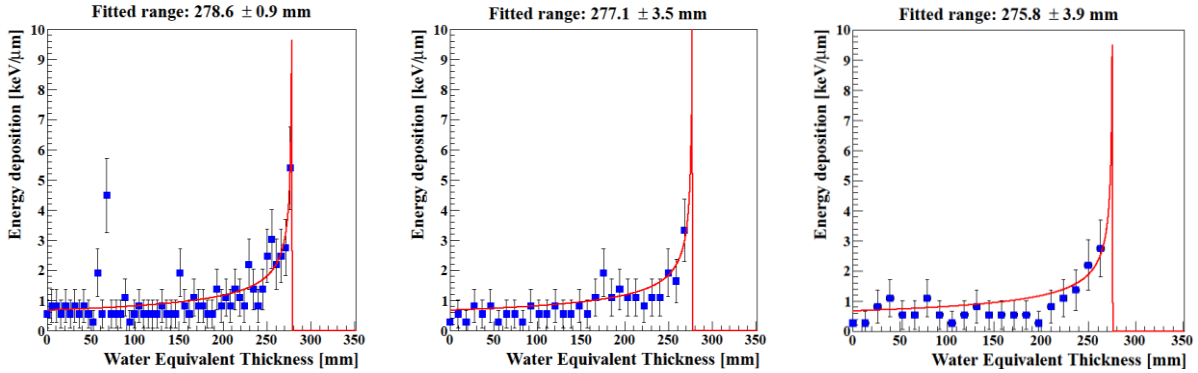

Figure 4: *Individual proton tracks with Bragg Curve fit. Note that the range found using thinner absorber designs yields a higher range determination accuracy. The displayed accuracy is the output from the least-squares method for an individual proton, and is not representative for an ensemble of protons. From a 250 MeV beam degraded using a 10 cm water phantom. Left: 2 mm Al absorber, Middle: 4 mm Al absorber, Right: 6 mm Al absorber.*

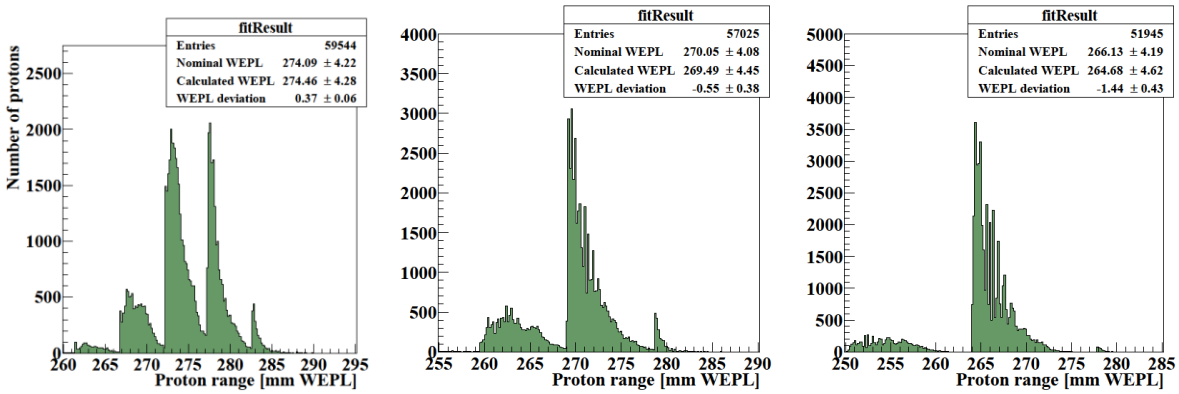

Figure 5: *The distribution of many individual fitted ranges. From this distribution the residual range* $\langle \boldsymbol{R_0} \rangle$ *and range straggling* $\langle \boldsymbol{\sigma} \rangle$ *of a proton ensemble is calculated, shown here as* $\langle \boldsymbol{R_0} \rangle \pm \langle \boldsymbol{\sigma} \rangle$*. Each rise in the distribution coincides with the beam reaching a new sensor layer. From a 250 MeV beam degraded using a 10 cm water phantom.* ***Left****: 2 mm Al absorber,* ***Middle****: 4 mm Al absorber,* ***Right****: 6 mm Al absorber.*

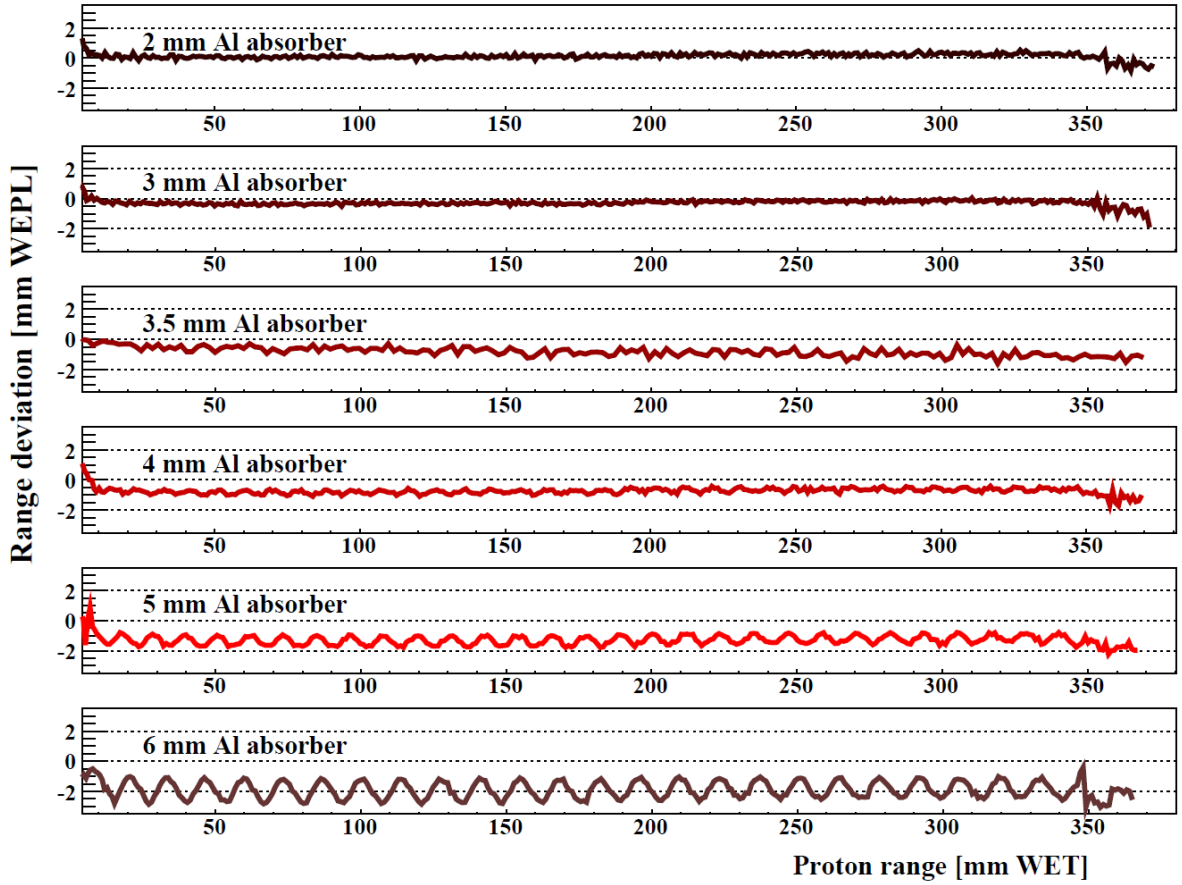

Figure 6: *Range determination accuracy shown as the deviation between the true (MC) range, and the reconstructed range* $\langle \boldsymbol{R_0} \rangle$ *for each water degrader thickness. In general the systematic errors are kept within 0.5 mm WET. An oscillating systematic error occurs when using thick absorbers due to the large spacing between the measurements in subsequent layers. The 3.5 mm figure has been produced with a somewhat lower statistical power, as can be seen in the noisier curve.*

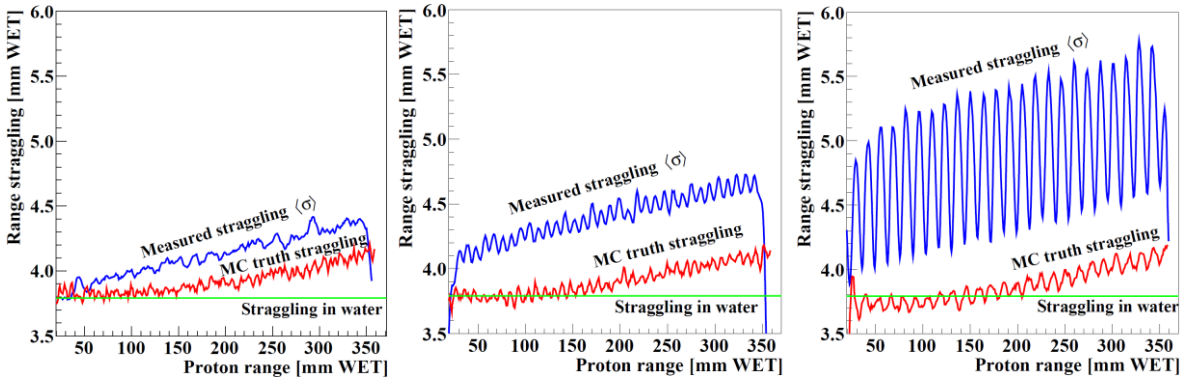

Figure 7: *The measured range straggling* $\langle\sigma\rangle$*, shown here together with the MC truth range straggling and the "baseline" range straggling in water. An oscillating systematic error occurs when using thick absorbers due to the large spacing between the measurements in subsequent layers.* ***Left:*** *2 mm Al absorber,* ***Middle:*** *4 mm Al absorber,* ***Right:*** *6 mm Al absorber.*

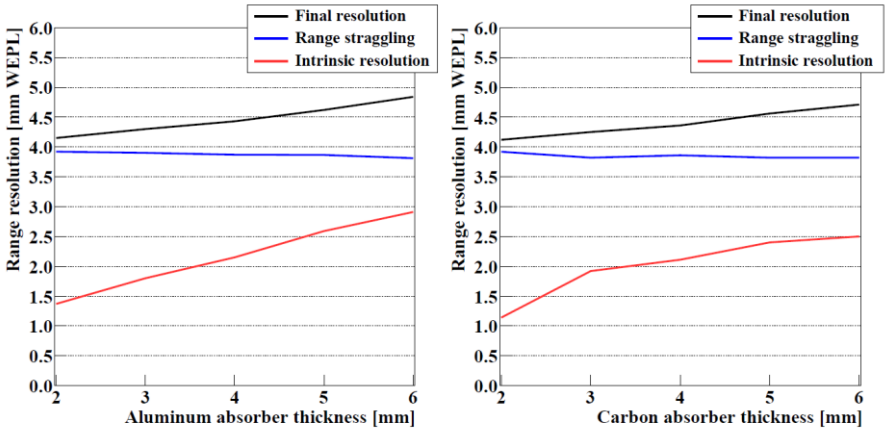

Figure 8: *Range resolution of the different configurations. Shown is the total resolution (measured as the mean value of* $\langle\sigma\rangle$ *in* ***Figure 6****), the range straggling from the MC truth as well as the intrinsic resolution which is the quadratic difference between the two.*

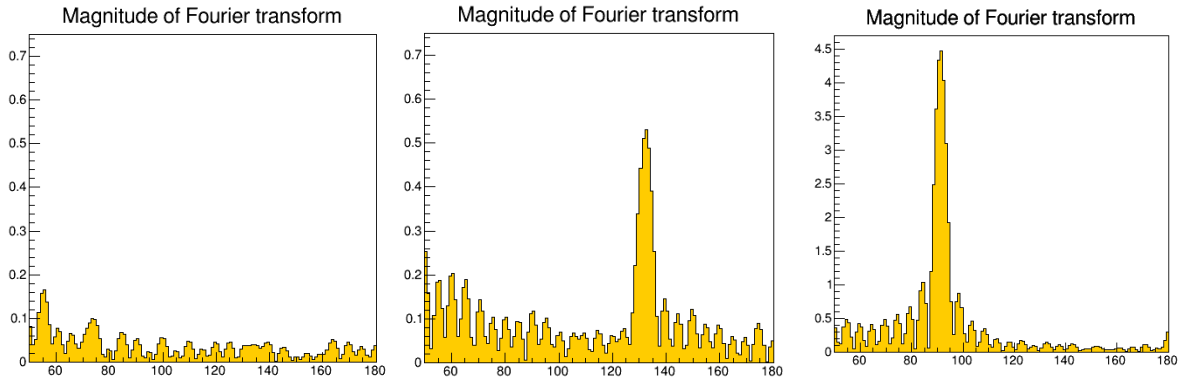

Figure 9: *The Fourier transform of 2 mm (****left****), 4 mm (****middle****) and 6 mm (right) absorber geometries. Compare this to* **Figure 6**, *where the wobbles are discernible: Here they are measurable.*

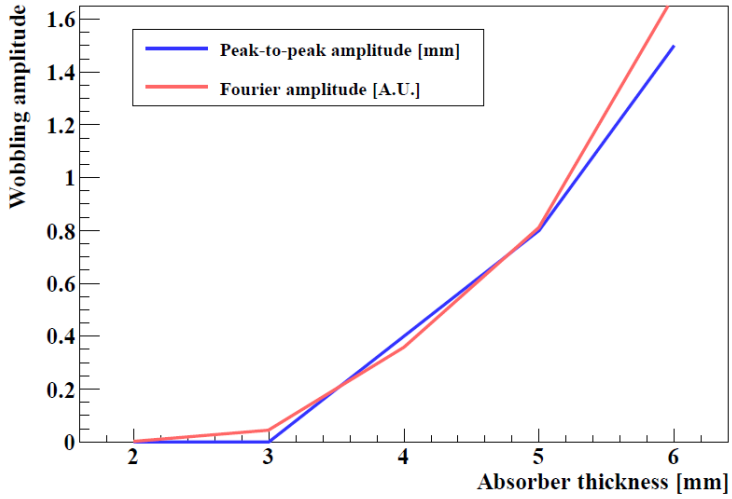

Figure 10 *Measurements of the peak-to-peak amplitude of the wobbles and the (artificially scaled) Fourier amplitude. X-axis is absorber thickness, Y-axis mm peak-to-peak. The measurements agree, and so it is trivial to quantify the amplitude of the oscillation artefacts.*

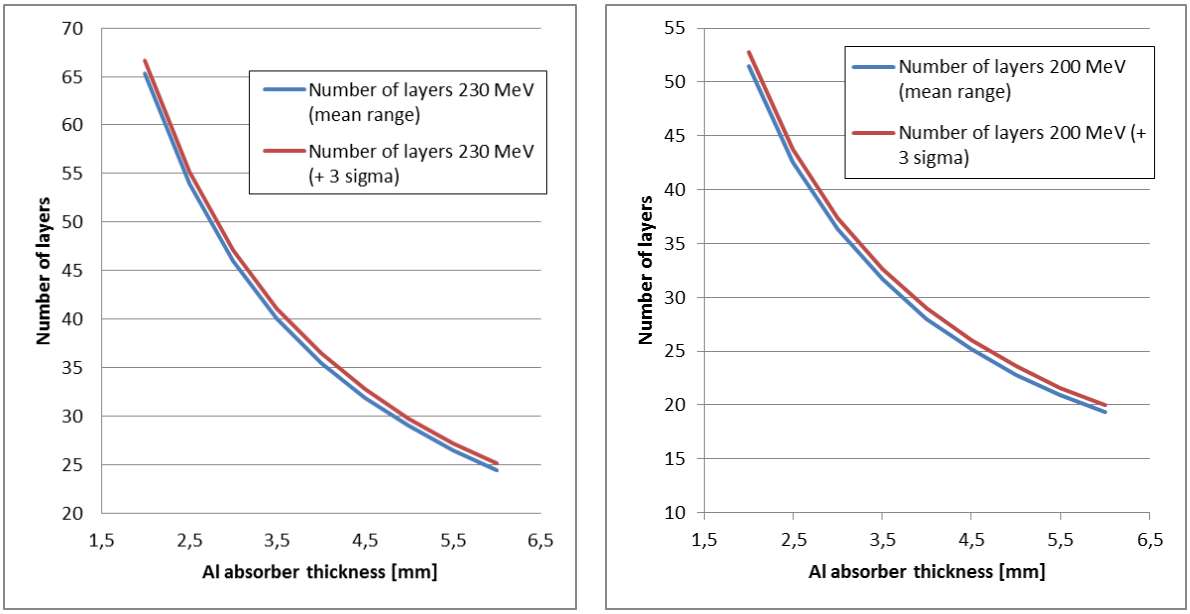

Figure 11 *Number of layers needed to contain a 230 (left) and 200 (right) MeV beam, with and without a 3 sigma range straggling addition.*

Absorber thickness [mm]	**2**	**2,5**	**3**	**3,5**	**4**	**4,5**	**5**	**5,5**	**6**
Layers 230 MeV (mean range)	65,3	54	46	40,1	35,5	31,9	29	26,5	24,4
Layers 230 MeV (+ 3 sigma)	66,6	55,2	47,1	41,1	36,5	32,8	29,7	27,2	25,1
Layers 200 MeV (mean range)	51,5	42,6	36,3	31,7	28	25,2	22,8	20,9	19,3
Layers 200 MeV (+ 3 sigma)	52,8	43,8	37,4	32,6	29	26	23,6	21,6	20

Table 1 *Number of layers needed to contain a 230 and 200 MeV beam, with and without a 3 sigma range straggling addition, for different absorber thicknesses.*

EFFICIENCY OF TRACK RECONSTRUCTION

The efficiency of the track reconstruction is shown in **Figure 3** for the 6 different designs considered in this work. The efficiency was calculated using a 100 cm^2 irradiation field and by varying the number of protons reconstructed simultaneously. For the 4 mm design, the efficiency is 90% at 4 protons per cm^2 per reconstruction frame, and 80% if the proton density is doubled. The results are the same for both aluminum and carbon absorbers.

ACCURACY OF THE RANGE CALCULATION

In **Figure 6** the range determination accuracy throughout the DTC is shown for the different designs. Some key aspects can be seen in the figure: The *systematic errors* are kept within 0.5 mm WET throughout the DTC for the designs having a 4 mm Al absorber or less, and higher for the designs with more than 4 mm Al absorbers. The *dynamic range* of the DTC, given by the region with uniform range uncertainty and uniform range accuracy, is approximately between 10 mm WET and 350 mm WET.

There is a certain oscillatory behavior in the range determination. This is especially more pronounced for the designs with absorbers having thicknesses of 4 mm and more. This is characterized by a sinusoidal perturbation of the range accuracy due to the sparse sampling of the layer measurements in depth. A Fourier analysis of the range accuracy has shown that this oscillation becomes significant (having a peak-to-peak amplitude of more than 0.25 mm WET) when an aluminum absorber thickness above 4.5 mm is used.

UNCERTAINTY OF INDIVIDUAL PROTON RANGE CALCULATION

The uncertainty of the range determination is highly dependent on its lower limit, which is the statistical range straggling of the proton beam. The resulting range uncertainty is a quadratic sum between the range straggling and the additional smearing due to detector geometry and analysis. As is apparent in **Figure 8**, the range straggling is dominated by the straggling induced by interactions in the water phantom, with an increase in the uncertainty for high energy protons traversing a higher fraction of the DTC material. The range straggling inhibits an oscillating systematic error with a period matching the spacing of the sensor layers.

THE ADDED SCATTERING FROM THE CARRIER BOARD AFTER THE FIRST LAYER

One of the required measurements during the proton CT image acquisition is that of the incoming proton vector. Any material in the first sensor layer (i.e. sensor chip, PCB and carrier backing material) will scattering the incoming protons with an RMS angle of $\Delta\theta_0$ found by the Highland eq.:

$$\Delta\theta_0 = \frac{14.1}{pv}\sqrt{\frac{d}{X_0}}\left(1 + \frac{1}{9}\log_{10}\left(\frac{d}{X_0}\right)\right)$$

We assume the scattering event to be happen near the first sensor layer[1] and the first sensor layer to be positioned 15 cm after the object (a slight increase compared to [2], however we want to spread the beam as much as possible before the calorimeter). Moreover, we simplify the geometry somewhat, so that the PCB is consisting of 40 µm Al and 60 µm Si and that the ALPIDE chip of 10 µm Al and 40

[1] A worst-case assumption, considering that the error would be smaller if the scattering happened before the first sensor layer (same angle error, less deflection distance) or after the first sensor layer (smaller scattering angle error measurement, same deflection distance). Moreover, the error is on the order of ~15 cm / 0.5 mm ~ 0.3%.

[2] Bopp et al., "The Impact of Tracking System Properties on the Most Likely Path Estimation in Proton CT."

µm Si. The carrier board of variable thickness is added to this. The degraded resolution is best calculating by performing a full Most Likely Path study, however is estimated by the proxy variable "RMS lateral deflection of proton vector on phantom". This variable should be kept as low as possible, and below 0.5 mm. This value is found by projecting $\Delta\theta_0$ onto the phantom 15 cm away. In **Figure 12** we see that the carrier board thickness should be kept below 450 µm Al in order for this constraint to be fulfilled.

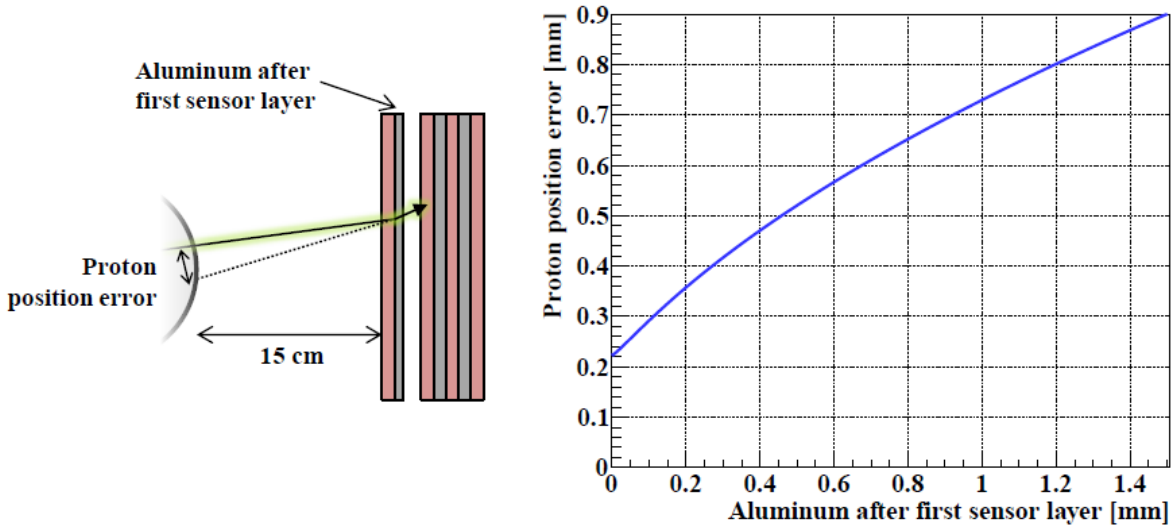

Figure 12: *Proton position determination error on phanom due to scattering in the ALPIDE chip, PCB and the added carrier board.* ***Left****: Schematics of the calculation.* ***Right:*** *Errors from different carrier board thicknesses.*

REQUIRED NUMBER OF SENSOR LAYERS

In this part of the analysis we do not as yet know all the details regarding the final design specifications of the DTC. Some assumptions have been made of the detector construction in the longitudinal dimension:

1. The sensor consists of 40 µm Si + 10 µm Al
2. The PCB is 130 µm thick (20% thinner than the MIMOSA23 prototype), but consisting of similar materials (Cu + SiO2 epoxy)
3. Ag glue (80 µm), same as MIMOSA23
4. Air gap of 2 mm between the layers – this is not vital to the results
5. The maximum beam energy is 230 MeV.

Using these assumptions, GATE simulations as well as calculations using the stopping power tables from PSTAR have been performed. The results are summarized in **Figure 11** and **Table 1**. In essence, using a 3.5 mm geometry, 41 layers would suffice to fully stop a 230 MeV proton beam in the detector.

Bopp, C, R Rescigno, M Rousseau, and D Brasse. “The Impact of Tracking System Properties on the Most Likely Path Estimation in Proton CT.” *Physics in Medicine and Biology* 59, no. 23 (December 7, 2014): N197–N210. https://doi.org/10.1088/0031-9155/59/23/N197.

Pettersen, H. E. S., J. Alme, A. Biegun, A. van den Brink, M. Chaar, D. Fehlker, I. Meric, et al. “Proton Tracking in a High-Granularity Digital Tracking Calorimeter for Proton CT Purposes.” *Nuclear Instruments and Methods in Physics Research Section A: Accelerators, Spectrometers, Detectors and Associated Equipment* 860C (2017): 51–61. https://doi.org/10.1016/j.nima.2017.02.007.

Pettersen, H. E. S., M. Chaar, I. Meric, O. H. Odland, J. R. Sølie, and D. Röhrich. “Accuracy of Parameterized Proton Range Models; a Comparison.” *Radiation Physics and Chemistry*, no. In press (n.d.).